Articles

2020

Towards a Rapid Screening of Liver Grafts at the Operating Room Using Mid-Infrared Spectroscopy

David Perezguaita
Technological University Dublin, david.perezguaita@tudublin.ie

Marta Moreno Torres
Unidad de Hepatología Experimental, Health Research Institute Hospital La Fe,

Ramiro Jover
Unidad de Hepatología Experimental, Health Research Institute Hospital La Fe,

See next page for additional authors

Recommended Citation

Authors

David Perezguaita, Marta Moreno Torres, Ramiro Jover, Eugenia Pareja, Bernard Lendl, Julia Kuligowsky, and Guillermo Quintas

Towards a rapid screening of liver grafts at the operating room using mid-infrared spectroscopy

SCHOLARONE™
Manuscripts

Towards a rapid screening of liver grafts at the operating room using mid-infrared spectroscopy

David Pérez-Guaita[a], Marta Moreno-Torres[b], Ramiro Jover[b,c,d], Eugenia Pareja[b,e], Bernhard Lendl[f], Julia Kuligowski[g*], Guillermo Quintás[h,i*], Jose Vicente Castell[b,c,d]

[a]*FOCAS Research Institute, Technological University Dublin, 13 Camden Row, D08CKP1, Dublin, Ireland*

[b]*Unidad de Hepatología Experimental, Health Research Institute Hospital La Fe, Av. Fernando Abril Martorell, 46026, Valencia, Spain*

[c]*Centro de Investigación Biomédica en Red de Enfermedades Hepáticas y Digestivas (CIBERehd), Instituto de Salud Carlos III, Av. de Monforte de Lemos 5. 28029, Madrid, Spain.*

[d]*Departamento de Bioquímica y Biología Molecular, Facultad de Medicina, Universidad de Valencia, Av. de Blasco Ibáñez, 15, 46010, Valencia, Spain*

[e]*Servicio de Cirugía General y Aparato Digestivo, Hospital Universitario Dr. Peset, Av. de Gaspar Aguilar, 90, 46017, Valencia, Spain*

[f]*Institute of Chemical Technologies and Analytics, Vienna University of Technology, Getreidemarkt 9/164, A 1060, Vienna, Austria*

[g]*Division of Neonatology, University & Polytechnic Hospital La Fe, Av. Fernando Abril Martorell, 46026, Valencia, Spain*

[h]*Unidad Analítica, Health Research Institute Hospital La Fe, Av. Fernando Abril Martorell, 46026, Valencia, Spain*

[i]*Health and Biomedicine, LEITAT Technological Center, Baldiri Reixac 10, 08028, Barcelona, Spain.*

KEYWORDS: lipidomics, liver, steatosis, infrared spectroscopy, ATR-FTIR, liquid chromatography – mass spectrometry.

Corresponding authors: Julia Kuligowski (Julia.kuligowski@uv.es), Guillermo Quintás (gquintas@leitat.org)

ABSTRACT: The estimation of steatosis in a liver graft is mandatory prior to liver transplantation, as the risk of graft failure increases with the level of infiltrated fat. However, the assessment of liver steatosis before transplantation is typically based on a qualitative or semi-quantitative characterization by visual inspection and palpation, and histological analysis. Thus, there is an unmet need for transplantation surgeons to have access to a diagnostic tool enabling an *in situ* fast classification of grafts prior extraction. In this study, we have assessed an Attenuated Total Reflection-Fourier Transform Infrared (ATR-FTIR) spectroscopic method compatible with the requirements of an operation room, for the evaluation of the lipid contents in human livers. A set of 20 human liver biopsies obtained from organs intended for transplantation were analyzed by expert pathologists, ATR-FTIR spectroscopy, lipid biochemical analysis, and UPLC-ESI(+/-)TOFMS for lipidomic profiling. Comparative analysis of multi-source data showed strong correlations between ATR-FTIR, clinical and lipidomic information. Results show that ATR-FTIR captures a global picture of the lipid composition of the liver, along with information for the quantification of the TAGs content in liver biopsies. Although the methodology performance needs to be further validated, results support the applicability of ATR-FTIR for the *in situ* determination of the grade of liver steatosis at the operation room as a fast, quantitative method, alternative to the qualitative and subjective pathological examination.

1. INTRODUCTION

Liver transplantation has become the therapy of choice for patients with irreversible end-stage liver diseases, being a lifesaving procedure for patients with acute liver failure[1]. The great success of this surgical procedure has led to an increasing demand for transplantable organs and a shortage of donor grafts to meet the demand which has led surgeons to consider suboptimal grafts. One of the most common disorders occurring in liver donors is non-alcoholic hepatic steatosis (NAFLD). Liver steatosis is typically characterized by the macro or microvesicular accumulation of lipid droplets within the cytoplasm[2] in the absence of a secondary contributing factor such as excess alcohol intake, viral infection, or drug treatments[3].

NAFLD is a challenging and multisystem disease that affects 25% of the global population[4]. It is qualitatively and semi-quantitatively evaluated by histological analysis under light microscopy of an extemporaneous biopsy. Thus, the surgeons extracting team at the site of organ donation, take the organ, prepare and preserve it for transportation to the hospital where the transplantation will take place, and while the recipient is being prepared for the surgery, the pathologist examines the graft to decide about its suitability. One of the reasons for rejecting the liver is an excess of fat accumulation.

1

Steatosis is nowadays highly prevalent, and the vast majority of liver donors do display this to a certain extent. Beyond a 50% volume of fat deposition within the cell, a liver graft tends to be rejected, and the operation has to be discontinued with the economic loses and the discomfort for the potential recipient. A way to minimize this would be an early estimation of the degree of steatosis, ideally at the site of organ extraction. The gold standard for the assessment of hepatic steatosis is a histological analysis by a pathologist describing semi-quantitatively the percentage of volume of hepatocytes containing lipid droplets in the cytoplasma[2]. Four grades of liver steatosis based on the percentage of fat within the hepatocytes have been proposed: grade 0 (no steatosis, <5%), grade 1 (mild, 5%-33%), grade 2 (moderate, 34%-66%), and grade 3 (severe, >66%)[3]. Histopathology also provides additional information about the occurrence of macro- or micro-steatosis, inflammation, ballooning degeneration and fibrosis. However, intra- and inter individual variability in interpreting images, the inconsistency of staining techniques, and sampling size errors may lead to a misrepresentation of the extent of steatosis. An additional limitation is that histological analysis does not provide information on the chemical composition of the lipids. Steatosis can also be graded by ultrasound or macroscopic evaluation during deceased donor procurement, but a previous study carried out in explanted, but not transplanted livers, showed that these procedures were not reliable[5]. Also, imaging techniques such as computed tomography or magnetic resonance imaging are rarely applicable to dead donors. Thus, there is an unmet need for transplantation surgeons to have analytical methods enabling a fast, *in situ* grading of liver steatosis prior to extraction.

Metabolomic characterization of lipid and phospholipid profiles using liquid chromatography – mass spectrometry (LC-MS) has shown that steatotic livers present high levels of cholesterol ester, diradylglycerols (DAGs), triradylglycerols (TAGs), free fatty acids, sphingolipids, and other lipids such as acylcarnitines and cardiolipins, compared to non-steatotic livers. On the contrary, certain phospholipids have lower concentrations in steatotic livers. Also, LC-MS and high-resolution magic-angle-spinning nuclear magnetic resonance based metabolomics have been used for the search of metabolomics signatures of graft dysfunction to forecast the outcomes before transplantation[6,7]. In spite of their relative high sensitivity and specificity, these techniques require time-consuming sample preparation and analysis, as well as data processing steps.

Fourier Transform Infrared (FTIR) spectroscopy is a label-free, non-destructive and cost-effective technique that provide molecular fingerprints of biological samples[8]. IR absorption can be associated with the concentration of biomolecules[9] (e.g., lipids, phospholipids, DNA, glycogen, proteins), informing on the global biochemical status of the cells within the tissue which could be exploited to evaluate tissue status and organ suitability[10]. FTIR-microspectroscopy has been proposed to grade steatosis on frozen tissue sections using standard[11] and synchrotron radiation[12,13] identifying differences in gluconeogenesis, glycolysis, and lipogenesis activities based on sugar and lipids contents in hepatocytes. FTIR spectra of unstained, frozen human liver tissue sections, acquired using a microscope, and Attenuated Total Reflectance (ATR)-FTIR spectra of frozen tissue sections deposited on a regular glass slide, showed that the average

lipids/proteins ratio measured by IR spectroscopy was linearly associated with the concentration of TAGs measured by gas chromatography-mass spectrometry[10]. ATR-FTIR was also recently used to quantify the degree of steatosis in freeze-dried liver tissue of a mouse model using the histological evaluation of liver sections as reference[14].

This study was undertaken as a proof of concept to evidence the potential of ATR-FTIR spectroscopy for rapid determination of the grade of liver steatosis and the lipid composition of human liver samples. Using reference information obtained from expert pathologists, total TAGs concentrations and LC-MS lipidomic profiles, our results demonstrate an excellent performance of dry film ATR-FTIR for a direct quantification of the TAGs content in liver biopsies, offering information to estimate relative lipid and phospholipid contents, and for the determination of the grade of liver steatosis. Further research will aim at the assessment of the applicability of ATR-FTIR for the *in situ* analysis of human livers at the operation room.

2. MATERIALS AND METHODS

Standards and reagents

LC-MS grade acetonitrile, isopropanol (IPA), methanol, and methyl tert-butyl ether (MTBE) were obtained from Scharlau (Barcelona, Spain) and formic acid (≥95%), and ammonium acetate (≥98%) from Sigma-Aldrich Química SL (Madrid, Spain). Ultra-pure water was generated employing a Milli-Q Integral Water Purification System (Merck Millipore, Darmstadt, Germany).

Samples

A total of 20 liver tissue samples were obtained from the Human Liver Collection at the BioBank of the University and Polytechnic Hospital La Fe (Valencia, Spain). This collection comes from donor livers which were primarily assigned to liver transplantation but, due to failings in some of the inclusion criteria (e.g. steatosis) they were donated to research. Liver samples were analyzed and classified according to histological information, the % macro and microsteatosis and the visual examination of the graft as 1: no steatosis; 2: low-intermediate steatosis; 3: intermediate-high steatosis; 4: high steatosis. The use of these samples for research purposes was approved by the Ethics Committee for Biomedical Research of the Health Research Institute La Fe (Valencia, Spain) (approval number 2014/0247).

Quantification of TAG in samples

A portion of 15-20 mg frozen liver tissue and 450 μL water were introduced in a 2 ml polypropylene tube containing CK14 ceramic beads (Precellys, France) for tissue homogenization (2 homogenization cycles of 25 s, 6,000 rpm, 5 °C) in a Precellys 24 Dual system. 400 μL were collected and mixed with 500 μL CH_3OH and 1 mL $CHCl_3$. The sample was homogeneized (vortex, 30 s), left on ice for 10 min, and centrifuged at 10,000 x *g* (15 min, 4°C). The lipid phase ($CHCl_3$) was collected, centrifuged (10,000 x *g*, 15 min, 4°C), evaporated to dryness and re-dissolved in 40 μL isopropanol. Total TAGs content was analyzed with a colorimetric kit (Spinreact, Barcelona, Spain). The TAG concentration in the sample was expressed as μg/mg protein[15].

ATR-FTIR analysis

Infrared spectra in the 3000 to 700 cm^{-1} range were acquired using a ReactIR15 FTIR (Mettler-Toledo, Columbus, USA)

spectrometer equipped with a liquid nitrogen-refrigerated mercury–cadmium–telluride detector. No purge system was required. Measurements were made using an AgX probe (9.5 mm x 1 m) accessory equipped with a diamond sensor composite (DiComp™) and a ZnSe focusing element for ATR, to simulate future experimental conditions in the operation room. A portion of ~5 mg of the liver sample was deposited in the center of the ATR crystal for the acquisition of the FTIR spectra of the tissue co-adding 256 scans with a resolution of 4 cm^{-1}. For the spectral acquisition of the dry film, a portion of ~5 mg of liver sample was deposited in the center of the ATR crystal and left for 15 s. Then, the sample was removed and 20 s after its removal, a spectrum of the dry residue was collected co-adding 256 scans with a resolution of 4 cm^{-1}. A spectrum of air previously recorded using the same instrumental conditions was used as background. The total measurement time was ~4 min/sample. After each measurement, the ATR surface was cleaned using a cotton swab and H_2O, isopropanol, CH_3OH and H_2O consecutively until recovery of the baseline signal. Spectral acquisition order was randomized to avoid biased results due to instrumental effects, but sample replicates were measured in a row to avoid additional tissue freeze and thaw cycles.

Lipidomic analysis

A portion of 20-40 mg frozen tissue was mixed with $CH_3Cl:CH_3OH$ (2:1) (20 µl/mg tissue) in a 2 ml polypropylene tube containing CK14 ceramic beads (Precellys, France) for tissue homogenization (3 homogenization cycles of 40 s at 6,000 rpm and 5 ºC, with pauses of 30 s between cycles) in a Precellys 24 Dual system (Precellys). Homogenates were collected and transferred to clean microcentrifuge vials for centrifugation (13,000 x g, 10 min, 4 ºC). Then, the supernatant was collected and 4 µl H_2O/mg tissue were added. The mixture was homogenized (vortex, 20s) and centrifuged (2,000 x g, 5 min, 4C). The organic phase was withdrawn and evaporated to dryness (SpeedVac). The residue was dissolved in 150 µl (1:1) (5:1:4 IPA:CH_3OH:H_2O, 5 mM CH_3COONH_4, 0.1% v/v HCOOH):(99:1 IPA:H_2O, 5 mM CH_3COONH_4, 0.1% v/v HCOOH). A blank extract was prepared following the same procedure but replacing tissue samples with water. For quality control, 10 µL of each sample extract were pooled in a glass vial to create a quality control (QC) sample.

Untargeted metabolomic analysis was carried out employing a 1290 Infinity ultra performance liquid chromatograph (UPLC) system from Agilent Technologies (CA, USA) equipped with a UPLC BEH C18 column (50 x 2.1 mm, 1.7 µm) from Waters (Wexford, Ireland). Full scan MS and MS^2 data in the range between 50 and 1500 m/z were acquired using an Agilent 6550 Spectrometer iFunnel quadrupole time-of-flight (QTOF) MS system. Samples were analyzed in two independent batches using positive and negative electrospray ionization (ESI+/-). Two blanks and nine QC replicates were injected at the beginning of each sequence for system conditioning and MS^2 data acquisition. Then, the sample batch including 20 liver samples in randomized order, 5 QCs (1 QC every 5 samples) and 5 blanks (2 before the first, and 3 after the last QC replicate) was analyzed. Blanks and QCs were used to monitor the instrument performance, correct within-batch effects, and identify unreliable, background, and carry-over features as described elsewhere[16],[17]. Iterated data dependent acquisition (DDA), in which MS^2 spectra were acquired in consecutive QC replicates using untargeted DDA

in the [70-200], [200-400], [400-600], [600-800], [800-1000], [1000-1250], and [1250-1500] Da ranges, was employed.

Peak table generation was carried out using XCMS[18]. The *centWave* method was used for peak detection with the following parameters: mass accuracy, 20 ppm; peak width, (3,15); snthresh, 50; prefilter, (5,3000); minimum difference in *m/z* for overlapping peaks, 10 mDa. Intensity weighted *m/z* values of each feature were calculated using the *wMean* function. Peak limits used for integration were found through descent on the Mexican hat filtered data. Grouping before and after RT correction was carried out using the *nearest* method and 9s as *rtCheck* argument and mzVsRTbalance = 5. Missing peaks were filled by reintegrating the raw data files using the *fillPeaks* method. The XCMS CAMERA package was used for the identification of pseudospectra across samples using *xsAnnotate*, *groupFWHM*, *findIsotopes*, *groupCorr* and *findAdducts* using standard parameters.

Automatic metabolite annotation was carried out as described elsewhere[19] using the following parameters: spectral libraries: HMDB (www.hmdb.ca) and LipidBlast; *m/z* accuracy in both, precursor and fragment ions (5 mDa); weight of *m/z* and intensity for the calculation of the *dot product* and *reverse dot product*[20] (in this study, m=1.2 and n=0.9 for *dp* and *rdp*, respectively); minimum number of matching ions in the experimental and reference spectra: 3; absolute and relative intensity thresholds in the MSMS spectra: 0.01% of the base peak and 200 AU; minimum *mean dot product:* 0.75. Metabolite annotation using LipidBlast was carried out using LipiDex using 0.01 Da tolerances in both MS (precursor) and MS^2 (fragment) data[20].

Software

Data acquisition and manual peak integration were carried out employing MassHunter Workstation (Agilent, version B.07.00). Raw data (.D) was converted into mzXML format using ProteoWizard (http://proteowizard.sourceforge.net/). Peak detection, integration, deconvolution, alignment and pseudospectra identification were carried out using XCMS and CAMERA in R 3.6.1. Principal Component Analysis (PCA) and Partial Least Squares (PLS) regressions were carried out in MATLAB 2020a (Mathworks Inc., Natick, USA) using in-house written scripts and the PLS Toolbox 8.7 (Eigenvector Research Inc., Wenatchee, USA). MATLAB scripts for Joint and Individual Variation Explained (JIVE) analysis were obtained from http://genome.unc.edu/jive. The LC-MS annotated peak table, ATR-FTIR and clinical data, MATLAB data and a .mlx MATLAB script are accessible at the Zenodo repository (DOI:10.5281/zenodo.3906954).

3. RESULTS AND DISCUSSION

Data overview

Figure 1 shows the ATR-FTIR spectra in the 1800-800 cm^{-1} range of four samples obtained during liver procurement for organ transplantation. Spectra were acquired after positioning each liver sample on top of the ATR surface (Figure 1A), and after removing the sample and waiting 20 s for the generation of the dry residue (Figure 1B). The figure also shows the spectra after standard normal variate (SNV) normalization using the standard deviation of each spectrum as normalization factor (see Figure 1C-D). In all cases, the main spectral contributions were derived from proteins, carbohydrates, phosphate bands from phospholipids, DNA and RNA, and lipids. Minor band shifts were observed between the spectra of

hydrated and dry samples. The intense and broad bands of water in the spectra of hydrated liver tissue samples strongly overlaps with other bands in the 1600-1700 cm^{-1} region, reducing the signal to noise ratio, and the repeatability of the measurements. Besides, previous works have reported that the extinction coefficients for the bands associated with the nucleic acids change with the hydration state, being assumed that similar effects could be valid for other biochemicals[21,22,23].

The bands at 1650 cm^{-1} (protein amide I), 1547 cm^{-1} (protein amide II), and 1309 cm^{-1} (protein amide III)[24] could be discerned in the absorbance spectrum of dry residues.
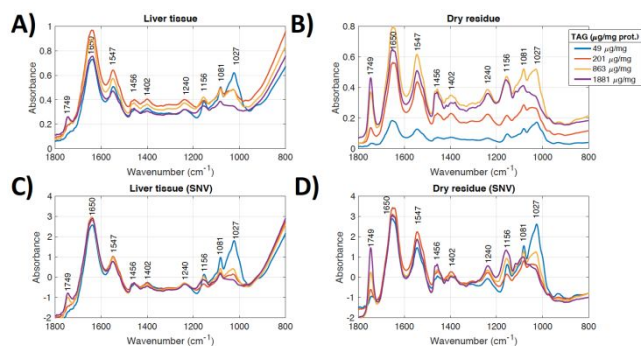

Figure 1. ATR-FTIR spectra of four liver tissues with different TAG concentrations in the 1800-800 cm^{-1} range. Spectra were acquired after positioning each liver sample on top of the ATR surface (A), and after removing the sample and waiting 20 s for the generation of the dry residue (B). Panels C and D show the A and B spectra after SNV normalization, respectively.

Characteristic bands associated with lipids at 1749 cm^{-1} (saturated ester C=O stretch from lipids and cholesterol esters), and 1456 cm^{-1} (CH$_2$ bending of lipidic acyl chains), 1402 cm^{-1} (COO- symmetric stretch of fatty acids and amino acids) were also present in the spectra. Furthermore, the 1300-900 cm^{-1} region contains overlapped bands from C-O and P-O stretching modes from lipids, phospholipids, carbohydrates and nucleic acids. Bands at 1240 cm^{-1} (PO$_2^-$ antisymmetric stretch from phospholipids[25] and nucleic acids[23]) and 1081 cm^{-1} (PO$_2^-$ symmetric stretch from phospholipids and nucleic acids) could be appreciated, as well as glycogen bands[26,27] at 1156 cm^{-1} (CO-O-C antisymmetric stretching of glycogen and nucleic acids) and 1027 cm^{-1} (C-O stretching of glycogen). The glycogen band at 1040 cm^{-1} overlap with the PO^{2-} band at 1081 cm^{-1}. Lipid bands at 2979 cm^{-1} (CH$_3$ asymmetric stretching), 2930 cm^{-1} (CH$_2$ antisymmetric stretch), and 2880 cm^{-1} (CH$_2$ symmetric stretch) showed low signal to noise ratio due to the intense absorption of the probe (AgX) in that region and were not displayed in Figure 1.
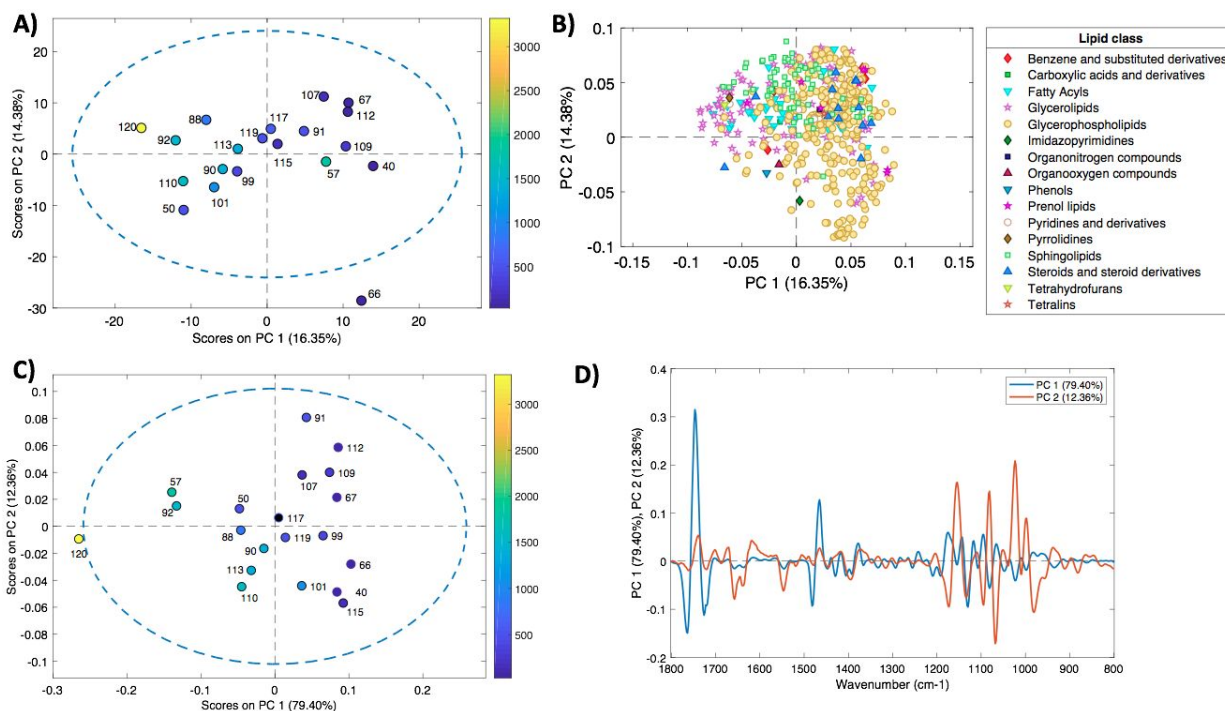

Figure 2. PCA scores (A,C) and loadings (B,D) plots obtained from the analysis of UPLC-TOFMS (top) and ATR-FTIR (bottom) data. Color scale in the scores plots indicates the reference TAGs concentration (µg/mg protein).

The comprehensive analysis of the hepatic lipidome is challenging. Nonetheless, the employed strategy for the lipidomic analysis of liver extracts by UPLC-TOFMS enabled the annotation of the major lipid classes (e.g. glycerophospholipids, glycerolipids, fatty acyls or sphingolipids) and subclasses (e.g. TAG, glycerophosphoethanolamines, glycerophosphocholines, glycerophosphoglycerols, or ceramides) constituents of liver (see Figure S1). Each of the 538 annotated features was

linearly correlated to the reference hepatic TAGs concentrations to get an overview about those changes in the lipidome associated with the grade of steatosis. Based on the ratio of annotated features with a statistically significant (p-value<0.05) linear association, four subclasses were inversely correlated to the TAGs content (glycerophosphoethanolamines, glycerophosphocholines, glycerophosphoinositoles, and glycerophosphoserines). On the other hand, triradylcglycerols, diradyglycerols, fatty alcohols

4

and linoleic acids and derivatives were mostly positively correlated to the reference TAGs concentrations (see Table 1)

Association between the ATR-FTIR spectra and the lipidomic profile.

The UPLC-TOFMS lipidomic and ATR-FTIR data sets were analyzed with PCA. Regarding the analysis UPLC-TOFMS data, the first two principal components (PCs) accounted for 16.4% and 14.4%, of the total variation in the autoscaled dataset, respectively. PC1 was associated with the relative TAGs content, indicating that this was one of the main sources of variation (see Figure 2A). Figure 2B shows the loadings plot with metabolites labelled according to their class for better visualization (a detailed version of the same plot displaying the subclasses can be found in the Figure S2).

The loadings plot indicated that glycerolipid (mainly TAGs and DAGs) and glycerophospholipid concentrations were inversely correlated, and that the ratio glycerolipids/glycerophospholipids was highly associated with the first PC. Distribution of samples along PC2 was partially linked to the relative concentrations of sphyngolipids, steroid and steroid derivatives and a group of glycerophospholipids with low loadings in PC2.

Table 1. Number of features (N) annotated according to the lipid class, and number of features showing a statistically significant positive (N^+) or negative (N^-) linear correlation with the TAGs content. Note: only subclasses with at least four annotated features were included. GPLs: Glycerophospholipids; GPEs: Glycerophosphoethanolamines; GPCs: Glycerophosphocholines; GPGs: Glycerophosphoglycerols; GPIs: Glycerophosphoinositols

Class	Subclass	N	N^+	N^-
GPLs	GPEs	80	2	5
Glycerolipids	Triradylcglycerols	63	18	7
GPLs	GPCs	60	1	6
GPLs	GPGs	60	4	2
Sphingolipids	Ceramides	59	2	0
Glycerolipids	Diradylglycerols	32	19	1
GPLs	GPIs	31	0	13
GPLs	Plasmenyl	31	2	6
Fatty acyls	Fatty acid esters	22	0	1
GPLs	Glycerophosphoserines	17	0	5
Sphingolipids	Glycosphingolipids	7	0	1
Fatty acyls	Fatty alcohols	6	3	0
Fatty acyls	Lineolic acids and deriv.	6	4	0
Steroids and deriv.	Cholestane steroids	4	1	1
Steroids and deriv.	Stigmastanes and deriv.	4	0	1

Figure 2C depicts the scores of the PCA model of the mean centered, normalized, derivative ATR-FTIR dataset. The use of the ATR-FTIR second derivative spectrum reduces the signal to noise ratio but it also eliminates spectral baseline shifts and enables a more specific identification of overlapping bands than in the original spectrum, thereby improving the specificity of the spectral analysis. PC1, accounting for 79.4% of the total variation, was again associated with the TAGs contents. Figure 2D showed that spectral regions associated

with lipid and phospholipids centered around 1749 and 1456 cm^{-1} presented higher loading values PC1. Considering the PCA was performed over the second derivative of the spectra, this implies that negative PC1 score values should be correlated with higher absorbance in these regions and hence with larger TAG content. This is in good agreement with results depicted in Figure 2C, showing an increasing of the TGAs levels when the PC1 score value decreases. The bands centered around 1152 and 1040 cm^{-1} attributed to glycogen and phospholipids showed high loadings in the second PC. Exploratory analysis by PCA pinpointed the glycerolipids concentration as one of the main sources of data variation and showed similar distributions of the samples in the PC1-PC2 scores space as those observed in the scores plot of UPLC-TOFMS data shown in Figure 2A. The Mantel test[28] was then applied to evaluate the correlation between the PCA scores plots obtained using ATR-FTIR and UPLC-TOFMS data. This test evaluates the significance of the correlation between pairwise distance matrices. In this study, the standardized Euclidean multivariate distances between matched sample pairs were used. The statistical significance of the Mantel test distance (r) was determined by a permutation test (10000 permutations). Results obtained demonstrated that both data sets were significantly related to each other (r = 0.30, p-value<0.001), showing the suitability of ATR-FTIR to capture complex biochemical information from liver samples.

JIVE is a chemometric approach suitable for the integration of multi-source data obtained from the same samples[29]. The algorithm identifies and separates the shared patterns among data sets (i.e. the joint structure, **J**) from the individual structure (**A**) of each data set that is unrelated to the joint structure. Here, JIVE split the data variation into low-rank approximations capturing variation across the ATR-FTIR and MS data sets (**J**), structured variation individual to ATR-FTIR and MS data sets (**A$_{IR}$** and **A$_{MS}$**), and the residual variations (**E$_{IR}$** and **E$_{MS}$**). After the selection of the ranks of **J** (r=2), **A$_{IR}$** (r=3) and **A$_{MS}$** (r=6) (significance threshold α=0.05, permutations: 1000, convergence threshold: 10^{-9}), the joint structure accounted for the 38% and 24% of the ATR-FTIR and MS variation, respectively, and the individual structures accounted for the 52% and 52% of the total variation in ATR-FTIR and MS, respectively (see Figure S3). The large contribution in **J** from ATR-FTIR data was in agreement with previous observations indicating that major changes in the liver composition observed by UPLC-TOFMS can be detected by ATR-FTIR.
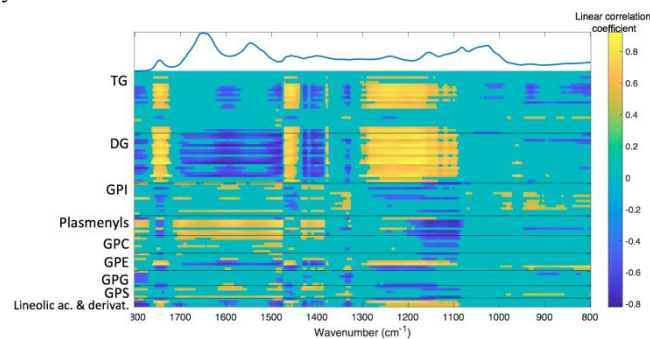

Figure 3. Correlations of LC-TOFMS lipid classes and ATR-FTIR data determined by heterospectroscopy using the Pearson coefficient. Notes: A correlation cutoff was applied (slope p-value<0.05) for a better visualization. TG: Tryglycerols; DG: Diglycerols; GPI: glycerophosphoinositols;

5

GPC: glycerophosphocholines; GPE: glycerophosphoethanolamines; GPS: glycerophosphoserines.

Joint comparative analysis of LC-MS and ATR-FTIR data

Statistical heterospectroscopy (HSY)[30] was employed to assess the correlation between IR bands and UPLC-MS data. In this study, HSY involved the calculation of the Pearson coefficient correlation between ATR-FTIR absorbances and the intensity of UPLC-MS features linearly correlated with the lipid content. From results depicted in Figure 3 two main patterns could be discerned: bands associated with neutral lipids centered on 1749 and 1456 cm^{-1}, and between 1300-1130 cm^{-1} presented statistically significant positive correlations with the concentrations of DAGs, TAGs and linoleic acids and derivatives lipid subclasses. On the contrary, bands centered around 1122 and 1100 cm^{-1} attributed to glycogen and phospholipids were mainly negatively correlated to plasmenyls and glycerophosphocholines concentrations. Patterns found in the HSY suggest a negative correlation between the glycerolipids and glycerohospholipids. Liver steatosis is characterized by an increase in intracellular fatty acid-derived metabolites (e.g. TAGs, DAGs) due to either increased uptake of free fatty acids and/or to up-regulated *de novo* hepatic lipogenesis[2]. Previous studies have reported decreased levels of phospholipids in steatosis[31].

Direct quantification of lipid content by ATR-FTIR spectroscopy

Figure 4A shows a statistically significant positive correlation between the intensity of the C=O(s) band at 1749 cm^{-1} in the normalized spectra and the TAGs contents in liver samples. Then, a multivariate PLS model was developed for the quantification of the relative TAGs content, using the 1800-800 cm^{-1} spectral region and SNV normalization. External validation is considered the gold standard to provide accurate prediction estimates of the generalization performance of predictive model. However, this approach requires the exclusion of test samples from the sample set used to develop the regression model. In this study, the number of samples was limited (n=20), and the selection of an external test set would have left too few calibration samples for being representative of the whole population. Thus, statistical validation was carried out by leave one out - cross validation (CV) and, to avoid overly optimistic results, no variable selection step was included during model development. Figure 4B shows the CV-predicted TAG concentrations using 2 latent variables providing a RMSECV = 316 µg/mg protein. The statistical significance of the model was assessed by permutation testing (250 permutations) as described elsewhere[32,33], providing a p-value<0.005 (see Figure 4C), thus indicating that the model was significant at the 95% confidence level. The analysis of the the contribution of the IR bands to the model was carried out considering the Variable Importance in Projection (VIP) and the regression vector, respectively. Figure 4D shows the spectrum of a liver sample with a color scale corresponding the VIP score value of each wavenumber. As expected, bands centered at 1749, 1456, and 1402 cm^{-1} associated with lipids show high positive values of the regression vector and VIP values.

Suitability of IR for steatosis quantitation

Liver tissues were classified into 4 categories based on the information provided by the pathologist, and on the reference TGA content using a 4-quantile clustering (1: no steatosis; 2:

low-intermediate grade; 3: intermediate-high steatosis; 4: high steatosis). Then, liver samples were classified based on the TAG content estimated by ATR-FTIR data and the quantiles defined by the reference TAGs values. Results showed, as expected, a good agreement between the classification provided by the pathologist and the TGA content, but also between the pathologist report and the classification estimated by ATR-FTIR. The slight differences in classification (e.g. 101 and 90, were classified as highly steatotic by the pathologist and TGA content, and as intermediate-high steatotic by ATR-FTIR), could be explained by the fact that the micro and macro steatosis which is easily observed under light microscopy, is composed principally by TGAs, while ATR-FTIR, provides a wider range of signals that include other lipids (e.g. sphyngolipids, glycerophospholipids) that cannot be accurately quantified under routine optical examination of tissue slices.

Table 2. Classification provided by the pathologists and the reference and predicted by ATR-FTIR relative TAGs concentrations (µg/mg protein). Grafts were classified according to the reference TAGs content using 4-quantile (q1-q4) clustering and 202, 560 and 1250 µg/mg protein as thresholds.

Graft #	Pathologist steat. class*	Reference TAG (q1-q4)	ATR-FTIR TAG (q1-q4)
112	1	30 (q1)	-18 (q1)
66	1	40 (q1)	463 (q2)
40	1	49 (q1)	503 (q2)
67	1	68 (q1)	227 (q2)
115	1	180 (q1)	316 (q2)
107	1	201 (q1)	531 (q2)
109	2	263 (q2)	144 (q1)
99	2	451 (q2)	250 (q2)
91	2	521 (q2)	127 (q1)
50	2	557 (q2)	1077 (q3)
119	3	506 (q2)	655 (q3)
117	3	660 (q3)	744 (q3)
88	3	863 (q3)	1171 (q3)
113	3	1360 (q3)	988 (q3)
101	4	1022 (q3)	618 (q3)
90	4	1370 (q4)	834 (q3)
92	4	1462 (q4)	1563 (q4)
110	4	1607 (q4)	1256 (q4)
57	4	1881 (q4)	1581 (q4)
120	4	3320 (q4)	3094 (q4)

*: Stratification based on the % macro and microsteatosis and on the visual examination of the graft. 1: no steatosis; 2: low-intermediate steatosis; 3: intermediate-high steatosis; 4: high steatosis.

Evaluation of the technique as a point of care tool

Results indicate that ATR-FTIR provides an overview of the lipid composition of the liver, as well as information for the quantification of the TAGs content and the grade of steatosis. However, liver tissue contains not only hepatocytes, but also

6

hepatic stellate cells, cholangiocytes, Kupffer cells and endothelial cells, and extracellular matrix. Thus, despite most of liver cells are hepatocytes, the biochemical composition reflects an average of all cells content in the liver biopsies, and may detract the correlation with the percentages of hepatocytes containing fat vacuoles in the cytoplasm estimated by histopathology. Also, although histopathological and IR analysis were performed on adjacent sections of the liver, the intrinsic liver heterogeneity may introduce a measurement error affecting the correlation between both techniques.

Data was acquired with the diamond IR sensor in direct contact with liver tissues. The liver is covered by a thin (~ 30-40 μm) layer of connective tissue fibers called Glisson's capsule composed primarily of type I collagen and, to a lesser extent, type III collagen. Collagens present a series of characteristic bands in the 1800-900 cm^{-1} range including amide I and II absorption bands at 1659 and 1555 cm^{-1}, bands at 1035 and 1079 cm^{-1} from the carbohydrate moieties, and at 1454, 1403, 1340, 1282, 1240, and 1205 cm^{-1} attributed to bending vibration of CH_2 and CH_3 groups as well C-N and N-H stretching vibrations[34]. Thus, it must be addressed whether the acquisition of ATR-FTIR spectra by direct contact on a whole liver organ and hence through the barrier that represents the Glisson's capsule, would impair the spectral lectures to such extent as to prevent the meaningful read outs to estimate the liver lipid contents, and whether further chemometric analysis would enable the removal of spectral interferences arising from the Glisson's capsule. Should this be the case, it would be then conceivable the use of a handy ATR-FTIR equipment at the operations room in the course of a liver explant for transplantation.
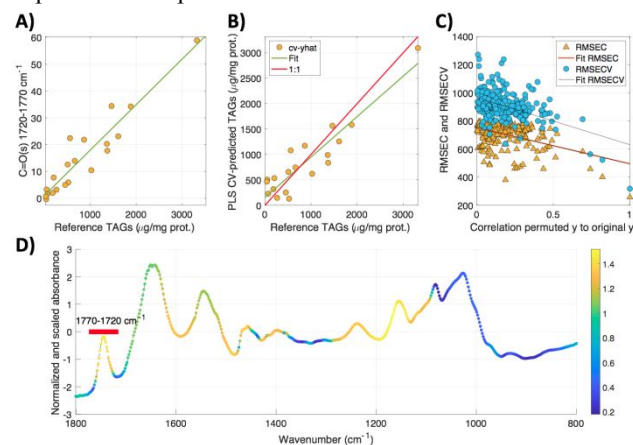

Figure 4. ATR-FTIR for the quantification of TAGs in liver samples. A) Linear regression between reference TAGs concentrations and ATR-FTIR band areas (1770-1720 cm^{-1}, two-points baseline: 1775, 1722 cm^{-1}); B) CV-PLS predicted TAG relative concentrations using the 1800 – 800 cm^{-1} region; C) Permutation test: assessment of the statistical significance of the RMSEC and RMSECV values; D) ATR-FTIR spectrum of a liver dry residue in the 1800-800 cm^{-1} range. The color scale indicates the VIP score in the PLS model build for the prediction of the TAGs concentrations.

4. CONCLUSIONS

This study is a proof of concept evidencing that ATR-FTIR renders valuable quantitative and qualitative descriptors of the lipid content of human liver biopsies. The acquisition of ATR-FTIR spectra can be rapidly carried out without complex sample processing or the use of toxic reagents, at virtually no cost, for a preliminary characterization of the lipid liver composition. The acquisition of dry film ATR-FTIR spectra is suitable for a fast determination of the grade of steatosis in liver grafts ready for transplantation. Although the methodology needs to be further validated, results indicate the potential applicability of ATR-FTIR as a point of care tool to support graft evaluation at the operation room.

ASSOCIATED CONTENT

Supporting Information

Figure S1. m/z-RT plot of the 704 annotated metabolites and pie chart summarizing the number of LC-TOFMS features annotated of each class.
Figure S2. PCA loading plots obtained from the analysis of LC-MS from lipidic extracts of liver samples representing all detected metabolite classes.
Figure S3. %Variation (sum of squares) explained by estimated Joint, Individual and residual structures

AUTHOR INFORMATION

Corresponding Authors

* Guillermo Quintás - *Health and Biomedicine, LEITAT Technological Center, Barcelona, Spain; Unidad Analítica, Health Research Institute Hospital La Fe, Valencia, Spain; orcid.org/0000-0002-4240-9846; e-mail: gquintas@leitat.org*
* Julia Kuligowski – *Neonatology research group, Health Research Institute Hospital La Fe, Valencia, Spain; orcid.org/ 0000-0001-6979-2235; e-mail: julia.kuligowski@uv.es*

Author Contributions

The manuscript was written through contributions of all authors. All authors have given approval to the final version of the manuscript.
Notes
The authors declare no competing financial interest.

REFERENCES

(1) Moon, D.-B.; Lee, S.-G. Liver Transplantation. *Gut Liver* **2009**, *3* (3), 145–165. https://doi.org/10.5009/gnl.2009.3.3.145.
(2) Engin, A. Non-Alcoholic Fatty Liver Disease. *Adv. Exp. Med. Biol.* **2017**, *960*, 443–467. https://doi.org/10.1007/978-3-319-48382-5_19.
(3) Nassir, F.; Rector, R. S.; Hammoud, G. M.; Ibdah, J. A. Pathogenesis and Prevention of Hepatic Steatosis. *Gastroenterol. Hepatol.* **2015**, *11* (3), 167–175.
(4) Younossi, Z. M.; Marchesini, G.; Pinto-Cortez, H.; Petta, S. Epidemiology of Nonalcoholic Fatty Liver Disease and Nonalcoholic Steatohepatitis: Implications for Liver Transplantation. *Transplantation* **2019**, *103* (1), 22–27. https://doi.org/10.1097/TP.0000000000002484.
(5) McCormack, L.; Dutkowski, P.; El-Badry, A. M.; Clavien, P.-A. Liver Transplantation Using Fatty Livers: Always Feasible? *J. Hepatol.* **2011**, *54* (5), 1055–1062. https://doi.org/10.1016/j.jhep.2010.11.004.

7

(6) Attard, J. A.; Dunn, W. B.; Mergental, H.; Mirza, D. F.; Afford, S. C.; Perera, M. T. P. R. Systematic Review: Clinical Metabolomics to Forecast Outcomes in Liver Transplantation Surgery. *Omics J. Integr. Biol.* **2019**, *23* (10), 463–476. https://doi.org/10.1089/omi.2019.0086.

(7) Faitot, F.; Besch, C.; Battini, S.; Ruhland, E.; Onea, M.; Addeo, P.; Woehl-Jaeglé, M.-L.; Ellero, B.; Bachellier, P.; Namer, I.-J. Impact of Real-Time Metabolomics in Liver Transplantation: Graft Evaluation and Donor-Recipient Matching. *J. Hepatol.* **2018**, *68* (4), 699–706. https://doi.org/10.1016/j.jhep.2017.11.022.

(8) Finlayson, D.; Rinaldi, C.; Baker, M. J. Is Infrared Spectroscopy Ready for the Clinic? *Anal. Chem.* **2019**, *91* (19), 12117–12128. https://doi.org/10.1021/acs.analchem.9b02280.

(9) Perez-Guaita, D.; Garrigues, S.; de la, M.; Guardia. Infrared-Based Quantification of Clinical Parameters. *TrAC Trends Anal. Chem.* **2014**, *62*, 93–105. https://doi.org/10.1016/j.trac.2014.06.012.

(10) Le Naour, F.; Gadea, L.; Danulot, M.; Yousef, I.; Vibert, E.; Wavelet, M.; Kaščáková, S.; Castaing, D.; Samuel, D.; Dumas, P.; Guettier, C. Quantitative Assessment of Liver Steatosis on Tissue Section Using Infrared Spectroscopy. *Gastroenterology* **2015**, *148* (2), 295–297. https://doi.org/10.1053/j.gastro.2014.11.038.

(11) Kochan, K.; Maslak, E.; Chlopicki, S.; Baranska, M. FT-IR Imaging for Quantitative Determination of Liver Fat Content in Non-Alcoholic Fatty Liver. *The Analyst* **2015**, *140* (15), 4997–5002. https://doi.org/10.1039/c5an00737b.

(12) Le Naour, F.; Bralet, M.-P.; Debois, D.; Sandt, C.; Guettier, C.; Dumas, P.; Brunelle, A.; Laprévote, O. Chemical Imaging on Liver Steatosis Using Synchrotron Infrared and ToF-SIMS Microspectroscopies. *PloS One* **2009**, *4* (10), e7408. https://doi.org/10.1371/journal.pone.0007408.

(13) Peng, C.; Chiappini, F.; Kaščáková, S.; Danulot, M.; Sandt, C.; Samuel, D.; Dumas, P.; Guettier, C.; Le Naour, F. Vibrational Signatures to Discriminate Liver Steatosis Grades. *The Analyst* **2015**, *140* (4), 1107–1118. https://doi.org/10.1039/c4an01679c.

(14) Szafraniec, E.; Tott, S.; Kus, E.; Augustynska, D.; Jasztal, A.; Filipek, A.; Chlopicki, S.; Baranska, M. Vibrational Spectroscopy-Based Quantification of Liver Steatosis. *Biochim. Biophys. Acta BBA - Mol. Basis Dis.* **2019**, *1865* (11), 165526. https://doi.org/10.1016/j.bbadis.2019.08.002.

(15) McMahon, A.; Lu, H.; Butovich, I. A. The Spectrophotometric Sulfo-Phospho-Vanillin Assessment of Total Lipids in Human Meibomian Gland Secretions. *Lipids* **2013**, *48* (5), 513–525. https://doi.org/10.1007/s11745-013-3755-9.

(16) Martínez-Sena, T.; Luongo, G.; Sanjuan-Herráez, D.; Castell, J. V.; Vento, M.; Quintás, G.; Kuligowski, J. Monitoring of System Conditioning after Blank Injections in Untargeted UPLC-MS Metabolomic Analysis. *Sci. Rep.* **2019**, *9* (1), 9822. https://doi.org/10.1038/s41598-019-46371-w.

(17) Kuligowski, J.; Sánchez-Illana, Á.; Sanjuán-Herráez, D.; Vento, M.; Quintás, G. Intra-Batch Effect Correction in Liquid Chromatography-Mass Spectrometry Using Quality Control Samples and Support Vector Regression (QC-SVRC). *The Analyst* **2015**, *140* (22), 7810–7817. https://doi.org/10.1039/c5an01638j.

(18) Smith, C. A.; Want, E. J.; O'Maille, G.; Abagyan, R.; Siuzdak, G. XCMS: Processing Mass Spectrometry Data for Metabolite Profiling Using Nonlinear Peak Alignment, Matching, and Identification. *Anal. Chem.* **2006**, *78* (3), 779–787. https://doi.org/10.1021/ac051437y.

(19) Ten-Doménech, I.; Martínez-Sena, T.; Moreno-Torres, M.; Sanjuan-Herráez, J. D.; Castell, J. V.; Parra-Llorca, A.; Vento, M.; Quintás, G.; Kuligowski, J. Comparing Targeted vs. Untargeted MS2 Data-Dependent Acquisition for Peak Annotation in LC-MS Metabolomics. *Metabolites* **2020**, *10* (4), 126. https://doi.org/10.3390/metabo10040126.

(20) Hutchins, P. D.; Russell, J. D.; Coon, J. J. LipiDex: An Integrated Software Package for High-Confidence Lipid Identification. *Cell Syst.* **2018**, *6* (5), 621-625.e5. https://doi.org/10.1016/j.cels.2018.03.011.

(21) Whelan, D. R.; Bambery, K. R.; Puskar, L.; McNaughton, D.; Wood, B. R. Synchrotron Fourier Transform Infrared (FTIR) Analysis of Single Living Cells Progressing through the Cell Cycle. *The Analyst* **2013**, *138* (14), 3891–3899. https://doi.org/10.1039/c3an00316g.

(22) Zohdi, V.; Whelan, D. R.; Wood, B. R.; Pearson, J. T.; Bambery, K. R.; Black, M. J. Importance of Tissue Preparation Methods in FTIR Micro-Spectroscopical Analysis of Biological Tissues: "Traps for New Users." *PloS One* **2015**, *10* (2), e0116491. https://doi.org/10.1371/journal.pone.0116491.

(23) Wood, B. R. The Importance of Hydration and DNA Conformation in Interpreting Infrared Spectra of Cells and Tissues. *Chem. Soc. Rev.* **2016**, *45* (7), 1980–1998. https://doi.org/10.1039/c5cs00511f.

(24) Cai, S.; Singh, B. R. A Distinct Utility of the Amide III Infrared Band for Secondary Structure Estimation of Aqueous Protein Solutions Using Partial Least Squares Methods. *Biochemistry* **2004**, *43* (9), 2541–2549. https://doi.org/10.1021/bi030149y.

(25) Perez-Guaita, D.; Sanchez-Illana, A.; Ventura-Gayete, J.; Garrigues, S.; de la Guardia, M. Chemometric Determination of Lipidic Parameters in Serum Using ATR Measurements of Dry Films of Solvent Extracts. *Analyst* **2014**, *139*, 170–178. https://doi.org/10.1039/c3an01057k.

(26) Apolonski, A.; Roy, S.; Lampe, R.; Maiti, K. S. Application of Vibrational Spectroscopy in Biology and Medicine. Breath Analysis. *Proceedings* **2019**, *27* (1), 26. https://doi.org/10.3390/proceedings2019027026.

(27) Toepel, J.; Welsh, E.; Summerfield, T. C.; Pakrasi, H. B.; Sherman, L. A. Differential Transcriptional Analysis of the Cyanobacterium Cyanothece Sp. Strain ATCC 51142 during Light-Dark and Continuous-Light Growth. *J. Bacteriol.* **2008**, *190* (11), 3904–3913. https://doi.org/10.1128/JB.00206-08.

(28) Mantel, N. The Detection of Disease Clustering and a Generalized Regression Approach. *Cancer Res.* **1967**, *27* (2), 209–220.

(29) Lock, E. F.; Hoadley, K. A.; Marron, J. S.; Nobel, A. B. JOINT AND INDIVIDUAL VARIATION EXPLAINED (JIVE) FOR INTEGRATED ANALYSIS OF MULTIPLE DATA TYPES. *Ann. Appl. Stat.* **2013**, *7* (1), 523–542. https://doi.org/10.1214/12-AOAS597.

(30) Crockford, D. J.; Holmes, E.; Lindon, J. C.; Plumb, R. S.; Zirah, S.; Bruce, S. J.; Rainville, P.; Stumpf, C. L.; Nicholson, J. K. Statistical Heterospectroscopy, an Approach to the Integrated Analysis of NMR and UPLC-MS Data Sets: Application in Metabonomic Toxicology Studies. *Anal. Chem.* **2006**, *78* (2), 363–371. https://doi.org/10.1021/ac051444m.

(31) Puri, P.; Baillie, R. A.; Wiest, M. M.; Mirshahi, F.; Choudhury, J.; Cheung, O.; Sargeant, C.; Contos, M. J.; Sanyal, A. J. A Lipidomic Analysis of Nonalcoholic Fatty Liver Disease. *Hepatol. Baltim. Md* **2007**, *46* (4), 1081–1090. https://doi.org/10.1002/hep.21763.

(32) Lloyd, G. R.; Hutchings, J.; Almond, L. M.; Barr, H.; Kendall, C.; Stone, N. Assessing the Performance of Spectroscopic Models for Cancer Diagnostics Using Cross-Validation and Permutation Testing; 2012; Vol. 8219, pp 82190C-82190C – 6. https://doi.org/10.1117/12.919864.

(33) Pérez-Guaita, D.; Kuligowski, J.; Garrigues, S.; Quintás, G.; Wood, B. R. Assessment of the Statistical Significance of Classifications in Infrared Spectroscopy Based Diagnostic Models. *Analyst* **2015**, *140* (7), 2422–2427. https://doi.org/10.1039/C4AN01783H.

(34) Belbachir, K.; Noreen, R.; Gouspillou, G.; Petibois, C. Collagen Types Analysis and Differentiation by FTIR Spectroscopy. *Anal. Bioanal. Chem.* **2009**, *395* (3), 829–837. https://doi.org/10.1007/s00216-009-3019-y.